



# Fast recovery of lead from hydrochloric acid via a novel silica-supported anion exchange resin for the determination of $^{210}\text{Pb}$ in environmental samples

Lifeng Chen<sup>a</sup>, Jie Zhang<sup>b</sup>, Xianwen He<sup>c</sup>, Manqing Liu<sup>c</sup>, Qiuyang Wei<sup>c</sup>, Xinpeng Wang<sup>b,\*</sup>, Yuezhou Wei<sup>a,b,\*</sup>

<sup>a</sup> School of Nuclear Science and Engineering, Shanghai Jiao Tong University, 800 Dong Chuan Road, Shanghai 200240, PR China

<sup>b</sup> School of Resources, Environment and Materials, Guangxi Key Laboratory of Processing for Non-ferrous Metallic and Featured Materials, Guangxi University, 100 Daxue Road, Nanning 530004, PR China

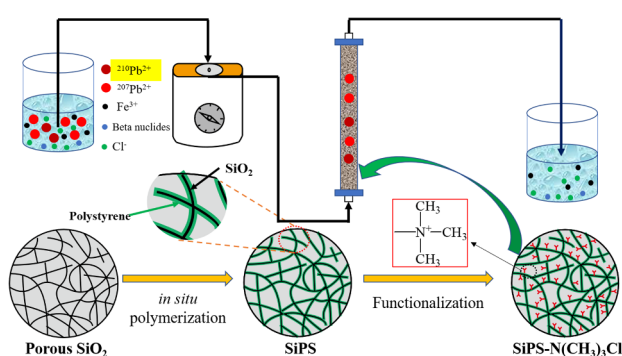
<sup>c</sup> Radiation-Environment Management and Monitoring Station of Guangxi Zhuang Autonomous Region, 80 Rong Mo Road, Nanning 530222, PR China



## HIGHLIGHTS

- A silica-supported anion exchanger was successfully synthesized and well characterized.
- The prepared material had almost no swelling and excellent adsorption kinetics.
- The adsorption behavior was well studied in the batch and column experiments.
- The time for lead separation was controlled within 30 min.
- The chemical yield of  $^{210}\text{Pb}$  exceeded 95%.

## GRAPHICAL ABSTRACT



## ARTICLE INFO

### Keywords:

Anion exchange  
Silica  
Lead-210  
Determination  
Adsorption kinetics

## ABSTRACT

The measurement of  $^{210}\text{Pb}$  is significant in environmental studies. Lead separation in HCl solution is a vital procedure but suffers from poor efficiency with high labor and time costs. To overcome this problem, a novel anion exchange resin was synthesized and characterized by different techniques followed by studies on the adsorption behaviors towards lead in HCl solution. The results suggest that SiPS-N(CH<sub>3</sub>)<sub>3</sub>Cl was successfully prepared with small particle size, low water swelling rate, and large specific surface area. The maximum anion exchange capacity resulted from quaternary amine groups was determined to be 1.0 mmol (Cl<sup>-</sup>)/g. The adsorption activities reached equilibrium within 5 min under selected conditions offering extremely fast adsorption kinetics. The synergistic adsorption mechanism and the competition from co-existing chloride anions were found to be responsible for the lead adsorption performance of SiPS-N(CH<sub>3</sub>)<sub>3</sub>Cl. Column experiments showed that the feeding volume of lead and HCl had impact on the chemical yield regardless of the co-existence of high concentrations of FeCl<sub>3</sub> (90 mM) and a high flow speed (4.0 mL/min). Based on these results, a separation process

\* Corresponding authors at: School of Nuclear Science and Engineering, Shanghai Jiao Tong University, 800 Dong Chuan Road, Shanghai 200240, PR China (Y. Wei).

E-mail addresses: [wangxinpeng@gxu.edu.cn](mailto:wangxinpeng@gxu.edu.cn) (X. Wang), [yzwei@sjtu.edu.cn](mailto:yzwei@sjtu.edu.cn) (Y. Wei).

<https://doi.org/10.1016/j.cej.2020.125300>

Received 1 February 2020; Received in revised form 28 April 2020; Accepted 29 April 2020

Available online 04 May 2020

1385-8947/ © 2020 Elsevier B.V. All rights reserved.

integrating SiPS-N(CH<sub>3</sub>)<sub>3</sub>Cl and the matched parameters was finally developed and tested. Our work greatly raised the lead separation efficiency in HCl solutions with implications for measuring <sup>210</sup>Pb in environmental samples.

## 1. Introduction

<sup>210</sup>Pb ( $t_{1/2} = 22.2$  y) is a radioactive isotope of stable <sup>207</sup>Pb that occurs naturally as one of the decay products of the <sup>238</sup>U series. Most <sup>210</sup>Pb is from <sup>222</sup>Rn ( $t_{1/2} = 3.8$  d) in the atmosphere or lithosphere after a series of decays (passing through <sup>218</sup>Po, <sup>214</sup>Pb, <sup>214</sup>Bi, and <sup>214</sup>Po). Other sources of <sup>210</sup>Pb include the burning of fossil fuels, the processing of lead ore, and car engines using tetraethyl lead as fuel [1]. <sup>210</sup>Pb leaves the atmosphere quickly by wet washout or dry deposition and readily enters soil or water [2,3]. The measurement of <sup>210</sup>Pb is significant for environmental studies, as it provides quantitative information on the flux of <sup>222</sup>Rn and its daughter nuclides in the atmosphere [4-6]. Such measurements are applied in uranium exploration, monitoring radionuclide migration in the uranium series, and luminescence dating of sediments [7-9]. <sup>210</sup>Pb and its daughter <sup>210</sup>Po have also aroused great public concern because they account for 35% of the total internal irradiation dose resulting from naturally occurring radionuclides. Such species can accumulate in foods especially seafoods and be ingested by humans [10-12]. The World Health Organization recommends that the activity concentration of <sup>210</sup>Pb be less than 0.1 Bq/L in drinking water [2].

The decay of <sup>210</sup>Pb is accompanied by the combined emission of beta particles (16 & 63 keV) and gamma rays (46.5 keV). It then transforms into <sup>210</sup>Bi (5.1 d), which next decays to <sup>210</sup>Po by emitting beta particles (1.2 MeV) [13]. The <sup>210</sup>Po is a pure alpha-emitter, and the emitted particle energy is 5.3 MeV. Traditional chemical analysis can't be used to detect the <sup>210</sup>Pb in the environmental samples, because the mass concentration is quite low and <sup>210</sup>Pb can't be distinguished from

other isotopes by instruments. Thus, the concentration of <sup>210</sup>Pb was always determined by the radioactive chemistry methods. Direct counting of beta particles emitted by <sup>210</sup>Pb is almost impossible due to the low energy. Generally, four main methods are used to determine <sup>210</sup>Pb including: (1) direct counting of gamma rays of <sup>210</sup>Pb [14], (2) separation of <sup>210</sup>Po followed by counting of its alpha activity [15,16], (3) separation of <sup>210</sup>Bi followed by counting its beta activity [17], and (4) separation of Pb followed by counting the beta activity of ingrowing <sup>210</sup>Bi [1,3,18]. These methods have both advantages and disadvantages.

Direct counting of gamma rays suffers from poor sensitivity and accuracy [1]. Method (2) has a long-time delay (at least 6 months) for the secular equilibrium <sup>210</sup>Pb-<sup>210</sup>Bi-<sup>210</sup>Po. It is also unable to obtain the chemical yield of Pb [19]. <sup>210</sup>Bi separation is selective and sensitive, but it requires equilibrium between <sup>210</sup>Pb and <sup>210</sup>Bi in samples and is not yet applicable for some biological and environmental samples [1]. Therefore, the separation of Pb followed by counting the beta activity of ingrowing <sup>210</sup>Bi is the most common method in the field of nuclide analysis due to its easy operation, rapid turnaround time, and excellent selectivity and accuracy.

Although the fourth method saves time versus other determination methods, significant time and labor are still required to separate lead. The brief separation flowsheet of <sup>210</sup>Pb is shown in Fig. 1, containing some procedures [20-22]: the addition of stable Pb as carrier, the co-precipitation with ferric hydroxide, the collection and dissolution of mixed precipitate, the lead purification (including adsorption and desorption) in columns, the evaporation of collected solution, the followed dissolution and final precipitate with sulphates, etc. As a vital procedure, column separation and evaporation occupy a large fraction

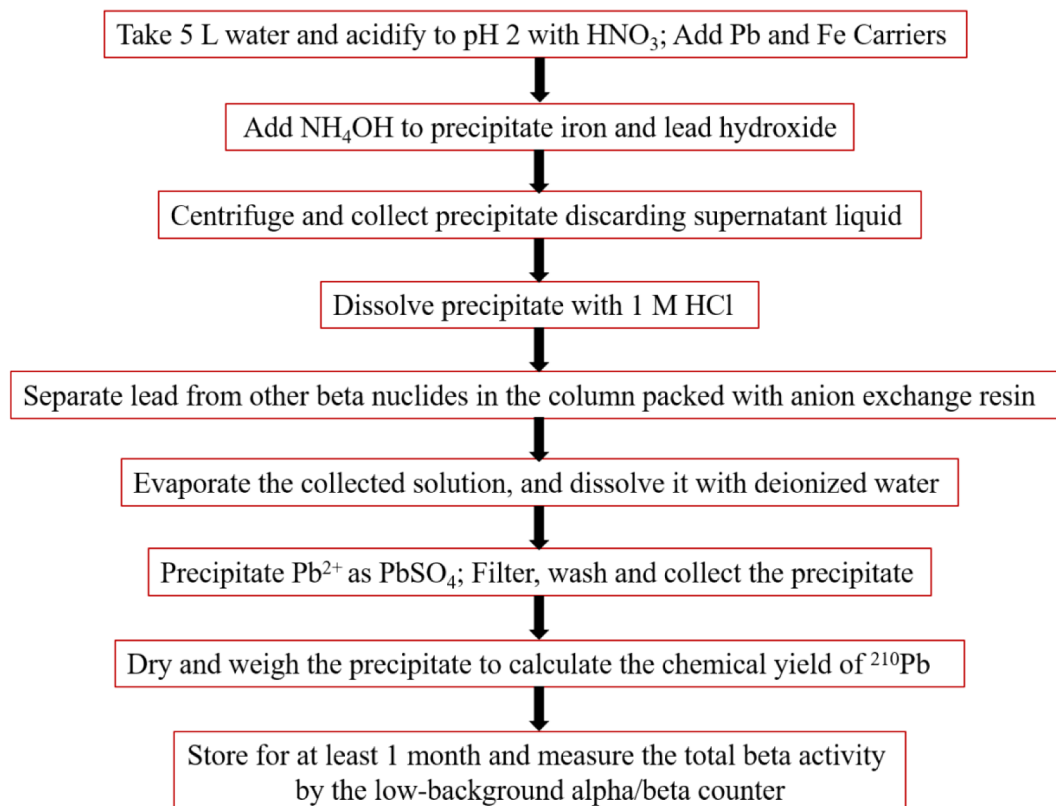


Fig. 1. The separation and purification flowsheet of <sup>210</sup>Pb.

of the total time and labor costs. The two procedures would last for several days for one sample assuming an 8-hour workday [21]. This is a common problem in radiation environmental monitoring; for example, in the Radiation/Environment Management and Monitoring Station of Guangxi Zhuang Autonomous Region and other similar governmental agencies situated in China. These agencies follow the same nuclear industry protocol originated from "Standard Test Method for Lead – 210 in Water" (ASTM D7535 – 2009).

Strong base anion exchange resins are commonly used to separate  $^{210}\text{Pb}$  such as Dowex1  $\times$  8 [7], BIO-RAD-AG 1-X4 [1], and 201  $\times$  7 [19]. The separation principle is that the lead cation can compound with chloride ions in the hydrochloric acid solution and then form anionic complexes that could be adsorbed by anion exchange resins; other metal cations like alkalis and alkaline earth metal cations cannot form such a complex. However, these resins suffer from poor adsorption kinetics [23–25], thus leading to a long separation time and low efficiency. More recently, scholars have developed lots of novel anion exchangers, such as cationic metal–organic framework materials (MOF) [26–29], cationic polymeric network materials [30], layered double-metal hydroxides materials (LDH) [31–33], inorganic cationic extended frameworks materials [34,35], and functionalized graphene oxide materials [36–38]. However, few works have investigated the separation and purification of lead in hydrochloric acid solution. Therefore, whether these anion exchangers could be used to separate  $^{210}\text{Pb}$  is unclear, especially because of the problematic chemical stability or column compatibility of these materials in strong acid. Here, we report the synthesis and characterization of a novel silica-supported anion

exchange resin with notable adsorption kinetics, extremely low swelling, and the same chemical properties as traditional anion exchange resins. The adsorption behaviors of this composite in hydrochloric acid were investigated in batch and column modes. As a result, a novel anion exchanger with excellent performance and a matched separation process with the optimum operation parameter were obtained. This system was used to separate lead from hydrochloric acid for downstream determination of  $^{210}\text{Pb}$  in environmental samples.

## 2. Experimental section

### 2.1. Materials and reagents

The silica used in the work was purchased from Fuji Silysia Chemical Ltd. (Japan). The particle size ranged from 75 to 150  $\mu\text{m}$ , and the porosity was 69%. The divinyl benzene (DVB) was a m/p-mixture stabilized with 1000 mg/L tert-butyl-catechol, and the purity was 55%, which needed to be purified by 1 M NaOH solution in advance to remove the stabilizer. DVB was purchased from Shanghai Aladdin Bio-Chem Technology Co., Ltd. and employed as a crosslinking agent. The initiator  $\alpha,\alpha'$ -azobisisobutyronitrile (AIBN; chemical purity) was obtained from Tianjin Guangfu Fine Chemical Research Institute. The chloromethyl methyl ether (CMME; analytical purity) was from Chengdu Aike Chemical Reagent Co., Ltd. and used as the chloromethylation reagent. The trimethylamine aqueous solution (TMA; 33 wt%) was purchased from Sinopharm Chemical Reagent Co., Ltd. and was used as the amination reagent. Other reagents were of

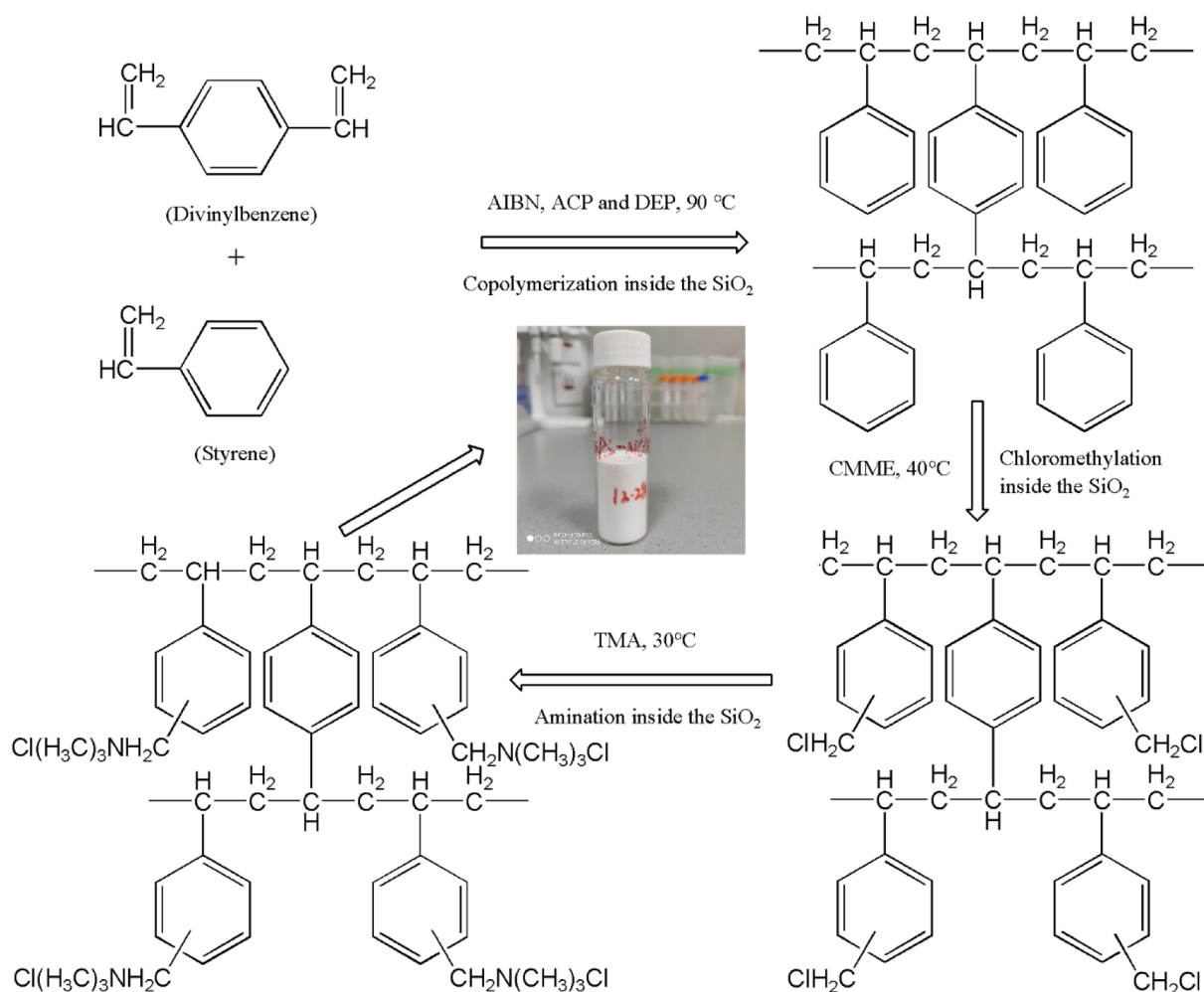


Fig. 2. The chemical reaction path for the synthesis of SiPS-N(CH<sub>3</sub>)<sub>3</sub>Cl.

analytical purity grade and were obtained from Shanghai Macklin Biochemical Co., Ltd., including styrene, zinc chloride, acetophenone, and diethyl phthalate (DEP), unless otherwise mentioned. All solutions were prepared with ultrapure water (UPW) with an electrical resistance > 18.2 M $\Omega$ . In this work, traditional resins, D201, 732, and IRA900, were used to compare with the synthesized materials and were purchased from Sunresin Company and Shanghai Macklin Biochemical Co., Ltd.

## 2.2. Synthesis

The silica-supported composite anion exchange resin was grafted with a quaternary amine group and was denoted as SiPS-N(CH<sub>3</sub>)<sub>3</sub>Cl. Fig. 2 shows the reaction path of preparation, which is separated into three main procedures:

### (1) Preparation of the silica-supported polystyrene (denoted as SiPS)

The synthesis of SiPS adopted an *in situ* solution copolymerization method where the DVB and styrene monomers were copolymerized in the mixed diluent of acetophenone and DEP without water. The mixed organic phase was sucked into the pores of silica particles via capillary and differential air pressure. A detailed synthesis has been published [39].

### (2) Chloromethylation of SiPS

Here, 40 g of SiPS and 120 mL of CMME were added to a three-neck flask fitted with a blender, an Allihn condenser, and a dripping funnel. The mixed phases were agitated slowly at room temperature for 3 h. Next, 7.2 g of ZnCl<sub>2</sub> was added in three batches. The flask was then heated in a water bath at 40 °C for 12 h. The stirring rate was controlled at 90–100 rpm, and the condensate temperature was 5 °C. After completing the reaction, the product was named SiPVBC (silica-supported poly-vinylbenzyl chloride) and was washed by UPW and ethanol and finally dried in a vacuum oven at 40 °C for 48 h. Before this procedure, the optimum ratio of catalyst to CMME was investigated to increase the chlorine content of SiPVBC (Fig. S1). The optimum ratio was then adopted.

### (3) The amination of SiPVBC

40 g of SiPVBC and 60 mL of benzene were added into a flask with three necks connected with a blender, an Allihn condenser, and a dropping funnel. The mixed phases were slowly stirred at room temperature for 4 h. Next, 100 mL of TMA was added into the flask dropwise at 10–20 °C within 6 h. The mixture was then heated in a water bath at 30 °C for 12 h after which 20 mL of additional TMA was added to continue the reaction for 2 h. The product was separated, washed by ethanol three times, and then placed in a saturated NaCl solution with pH adjusted to 2–3. After 2 h, the saturated NaCl solution was gradually diluted. The composite resin was then washed by UPW and finally dried in a vacuum oven at 40 °C for 48 h before use. The product was denoted as SiPS-N(CH<sub>3</sub>)<sub>3</sub>Cl.

## 2.3. Characterization

These prepared materials were characterized by FT-IR (Shimadzu IR Tracer 100, Japan), TG-DSC (Netzsch STA 449F3, Germany), SEM-EDS (Phenom Prox, Holland), BET (TRISTAR II 3020, United States), and elemental analysis (EA, Elementar Vario MICRO cube, Germany). For FT-IR, the spectrum was scanned from 400 cm<sup>-1</sup> to 4000 cm<sup>-1</sup> via a KBr disc. The TG-DSC analysis was conducted in an oxygen atmosphere at a flow rate of 20 mL/min and a heating rate of 5 °C/min. For SEM-EDS, the cross section was obtained by immobilizing the composite particles with acrylic resin.

## 2.4. The estimation of swelling rate

Traditional resins D201, 732, and IRA900 were compared with SiPS-N(CH<sub>3</sub>)<sub>3</sub>Cl for the bulk density and swelling rate. D201, 732, and IRA900 were pretreated according to the national standard of China GBT5476-1996. Finally, D201 and IRA900 were transformed into Cl-type, and 732 was transformed into Na-type. Next, the apparent volumes per unit mass were measured in a graduated cylinder as described previously [39]. The water swelling rate was estimated as the following equations:

$$S = (V_w - V_d)/V_d \times 100\%$$

where  $S$  (%) represents the water swelling rate,  $V_w$  (mL/g) and  $V_d$  (mL/g) are the apparent volume per unit mass at a wet and dry state, respectively.

## 2.5. The determination of amine groups

Next, 0.1026 g of SiPS-N(CH<sub>3</sub>)<sub>3</sub>Cl was packed in a glass column ( $\phi \times h = 5 \text{ mm} \times 10 \text{ cm}$ ). The column was first fed with 50 mL of UPW (this was discarded), and then eluted by 50 mL of 0.1 M NaNO<sub>3</sub> (collected). The amount of chloride ions in the effluent was measured with an ion chromatograph (Metrohm 930, Switzerland). Considering that the amine groups have a high affinity towards ReO<sub>4</sub><sup>-</sup>, the maximum adsorption amount towards the perchlorate anion was further measured by ICP-AES (Shimadzu S7510, Japan). The results suggested that the amount of chloride taken by SiPS-N(CH<sub>3</sub>)<sub>3</sub>Cl and the maximum exchange capacity were both about 1.0 mmol/g.

## 2.6. The calculation of lead species

The distribution of lead species was calculated by the PHREEQC software developed by the United States Geological Survey [40]. The thermodynamic data in the database PHREEQC.dat were employed and listed in Table S1.

## 2.7. Batch experiments

The 5000 mg (Pb<sup>2+</sup>)/L stock solution was prepared by dissolving 0.7993 g Pb(NO<sub>3</sub>)<sub>2</sub> in 100 mL of UPW. The working solution of 500 mg (Pb<sup>2+</sup>)/L was obtained by diluting the stock solution 10-fold. Other stock or working solutions were prepared as mentioned above. The 0.1 g of SiPS-N(CH<sub>3</sub>)<sub>3</sub>Cl was mixed with 5 mL of working solution in glass bottles. These bottles were covered with Teflon caps and placed in a shaker at room temperature; the shaking frequency was 120 rpm. These solutions were subsequently separated by the syringe filter with a mean pore size of 0.45  $\mu\text{m}$ . The separated solutions were diluted by 1%(v/v) HCl solution and measured by an atomic absorption spectrophotometer (AAS, Jena contra 700, Germany). The adsorption efficiency and amount were calculated via following two equations:

$$Q_e = (C_0 - C_e) \cdot V/m \quad (1)$$

$$D = (C_0 - C_e)/C_0 \times 100\% \quad (2)$$

Here,  $Q_e$  (mg/g) and  $D$  (%) are the adsorption amount and adsorption efficiency at the equilibrium state, respectively;  $C_0$  (mg/L) and  $C_e$  (mg/L) represent the initial and equilibrium concentration of lead, respectively;  $V$  (mL) is the volume of solution; and  $m$  (g) is the mass of the adsorbent.

The impact of initial concentrations of HCl and co-existing FeCl<sub>3</sub> were investigated to explore the adsorption behaviors of SiPS-N(CH<sub>3</sub>)<sub>3</sub>Cl towards lead cations in the HCl. In addition, the adsorption kinetics and isotherms were carefully studied by varying the contact time and the initial concentration of lead, respectively. Here, the pseudo-first order kinetic model (PSO), the pseudo-second-order kinetic model (PFO) and the intra-particle diffusion model were employed to fit

the kinetic data (see [Supporting Material \(S2\)](#)).

## 2.8. Column experiments

The 3.3579 g of SiPS-N(CH<sub>3</sub>)<sub>3</sub>Cl was packed in a glass column ( $\phi \times h = 5 \text{ mm} \times 30 \text{ cm}$ ) connected with a peristaltic pump (EYELA MP 2000, Japan) and an automatic fraction collector (EYELA DC-1500C, Japan); the dead volume was about 5.4 mL. The solution was pumped into the column at a certain speed and then collected by an automatic fraction collector. The column was regenerated by 30 mL UPW and pretreated with 20 mL of HCl (1.0 M) for the next experiment. Namely, the column was used repeatedly. Generally, four column experiments were performed with different aims (see [Supporting Material \(S3\)](#)).

## 3. Results and discussion

### 3.1. Characterization

The prepared samples were first characterized by TG-DSC analysis. Based on the weight loss, the organic percent of SiPS, SiPVBC, and SiPS-N(CH<sub>3</sub>)<sub>3</sub>Cl were 17.6%, 19.5%, and 24.6%, respectively ([Fig. 3](#)). The increased organic percent implied effective modification of the precursors. SiPS went through two apparent weight loss stages as the temperature increased from 25 to 650 °C. These stages were accompanied by two exothermic peaks near 311 and 491 °C, respectively, as shown in [Fig. 3\(a\)](#). The two weight loss stages both resulted from the decomposition of the organic bone structure. Compared to SiPS, SiPVBC appeared to have two weight loss stages as shown in [Fig. 3\(b\)](#). However, an exothermic shoulder peak occurred at about 256 °C in the DSC curve, which could be ascribed to the decomposition of the chloromethyl group. For SiPS-N(CH<sub>3</sub>)<sub>3</sub>Cl ([Fig. 3\(c\)](#)), two endothermic and four exothermic peaks appeared with the decomposition process. The first stage started from 25 °C to 139 °C, which could be attributed to the evaporation of residual water and the loss of methyl on quaternary

**Table 1**

The mass percent of N/C/H of different samples.

Sample Name	N (%)	C (%)	H (%)
SiPS	0	15.50	1.35
SiPVBC	0.055	15.545	1.2485
SiPS-N(CH <sub>3</sub> ) <sub>3</sub> Cl	1.30	17.21	2.43

amine groups based on the endothermic essence. The second weight loss stage occurred from 152 °C to 240 °C. This stage was also endothermic and could be ascribed to the thermal decomposition of the tertiary amine. The weight loss stages higher than 240 °C were the oxygenolysis of the organic bone structure. These were supported by the TG-DSC curves of the traditional organic resin D201 ([Fig. 3\(d\)](#)). The decomposition temperature points of D201 were different from those in SiPS-N(CH<sub>3</sub>)<sub>3</sub>Cl due to the differences in the degree of crosslinking and preparation technology. However, the order of decomposition should be consistent.

Elemental analysis was next used to acquire the mass percent of C/H/N. [Table 1](#) shows the analysis results of SiPS, SiPVBC, and SiPS-N(CH<sub>3</sub>)<sub>3</sub>Cl. The mass percent of nitrogen reached 1.3% after the amination of SiPVBC, which is equal to 0.93 mmol (N)/g (SiPS-N(CH<sub>3</sub>)<sub>3</sub>Cl). This is close to the results obtained in [Section 2.5](#), which suggests that the maximum exchange capacity resulted from quaternary amine was about 1.0 mmol (Cl<sup>-</sup>)/g. These results combined with the thermal analysis mentioned above indicated the successful preparation of the silica-supported anion exchange resin.

To obtain the information on pore structure, the resulting composite resin was further characterized by BET. [Fig. 4\(a\)](#) shows the nitrogen adsorption and desorption isotherms. The nitrogen adsorption and desorption isotherms produced an IUPAC type H1 hysteresis loop indicating a narrow pore diameter distribution and uniform shape of SiPS-N(CH<sub>3</sub>)<sub>3</sub>Cl. These findings are supported by the results in [Fig. 4\(b\)](#), suggesting that the pore diameter was mainly concentrated in the range of 10 nm to 70 nm; the micropores and macropores only

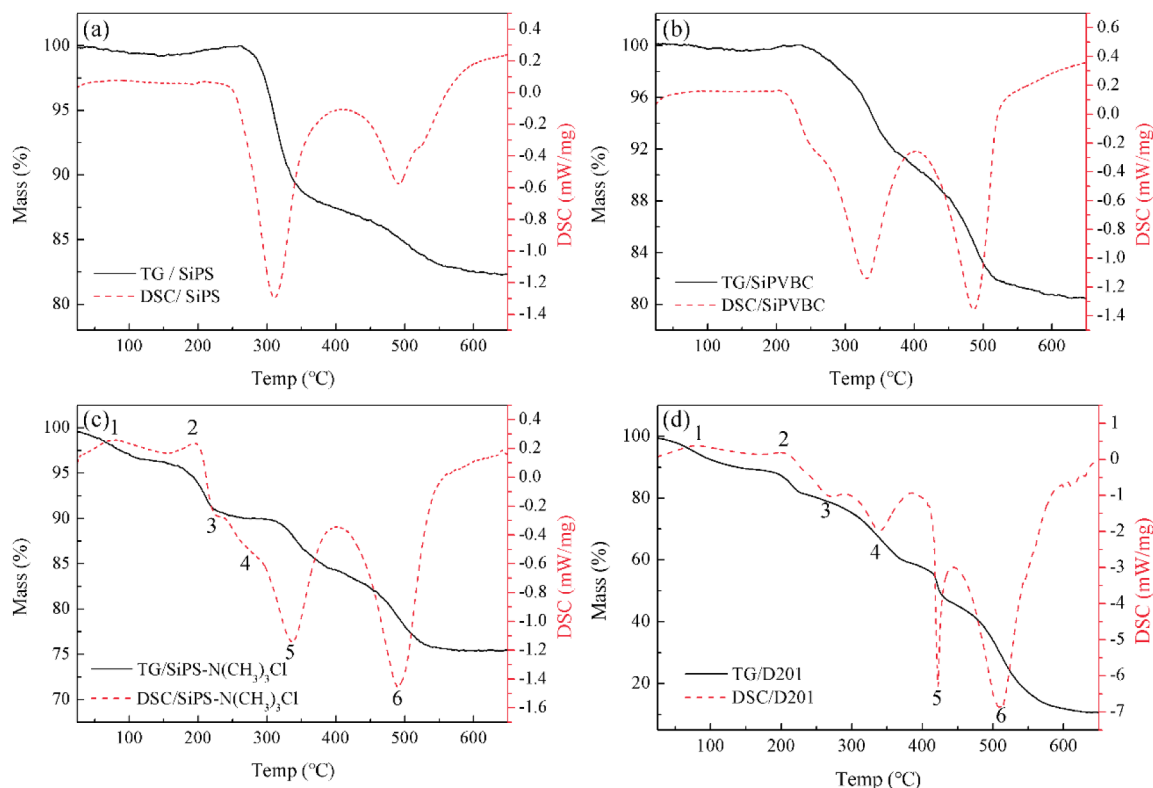


**Fig. 3.** The TG-DSC curves of SiPS, SiPVBC, SiPS-N(CH<sub>3</sub>)<sub>3</sub>Cl, and D201.

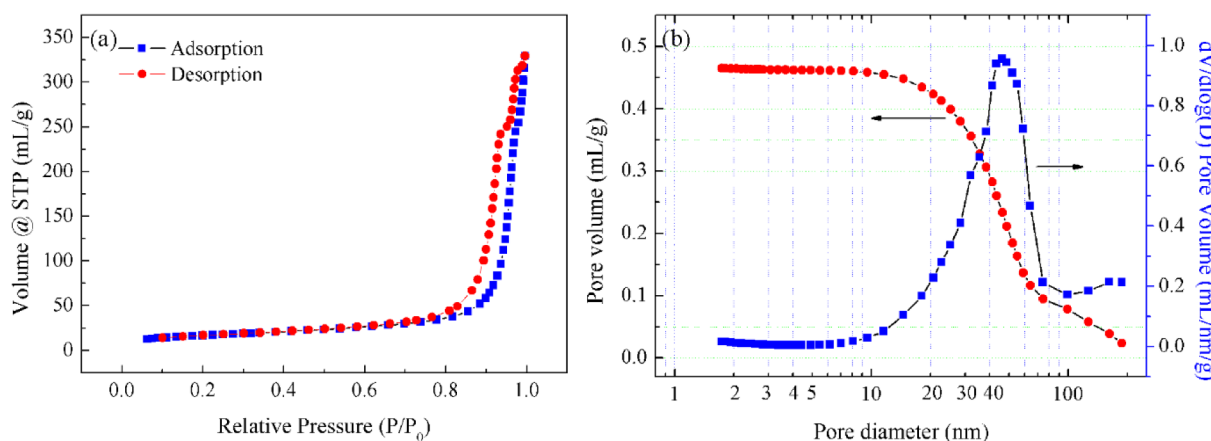


Fig. 4. Nitrogen adsorption and desorption isotherms (a) and the pore diameter distribution (b) of SiPS-N(CH<sub>3</sub>)<sub>3</sub>Cl.

Table 2

The parameters of pore structure for different materials.

Sample name	BET surface area (m <sup>2</sup> /g)	Pore volume (mL/g)	Average pore diameter (nm)
SiO <sub>2</sub> [25]	80.4	1.02	50.3
SiPS	95.72	0.6158	26.20
SiPS-N(CH <sub>3</sub> ) <sub>3</sub> Cl	59.03	0.4651	32.58

occupied a small portion. The pore parameters obtained by the BET analysis are reported in Table 2. The pore volume decreased from SiO<sub>2</sub> to SiPS to SiPS-N(CH<sub>3</sub>)<sub>3</sub>Cl due to the increased organic components. The BET surface area of SiPS-N(CH<sub>3</sub>)<sub>3</sub>Cl was 59.03 m<sup>2</sup>/g, which was much larger than that of traditional resin 732 (2.82 m<sup>2</sup>/g) and IRA900 (7.21 m<sup>2</sup>/g) [39]. The average pore diameter was 32.58 nm, suggesting that SiPS-N(CH<sub>3</sub>)<sub>3</sub>Cl was mesoporous. Generally, the implantation of the silica framework and the *in-situ* solution polymerization method gives this material possess a large specific surface area that is rich in pore structure.

To demonstrate that SiPS-N(CH<sub>3</sub>)<sub>3</sub>Cl had anion exchange capability, 1 M NaNO<sub>3</sub> solution was used to transform the SiPS-N(CH<sub>3</sub>)<sub>3</sub>Cl resin into the SiPS-N(CH<sub>3</sub>)<sub>3</sub>NO<sub>3</sub> type. The SiPS-N(CH<sub>3</sub>)<sub>3</sub>NO<sub>3</sub> was then exchanged with ReO<sub>4</sub><sup>-</sup> anions. SiPS-N(CH<sub>3</sub>)<sub>3</sub>NO<sub>3</sub> and the ReO<sub>4</sub><sup>-</sup>-loaded control were both washed with copious water in the columns and finally prepared into KBr pellets with SiO<sub>2</sub> and SiPS-N(CH<sub>3</sub>)<sub>3</sub>Cl for FT-IR characterization (Fig. 5).

SiPS-N(CH<sub>3</sub>)<sub>3</sub>Cl exhibited almost the same characteristic peaks as SiO<sub>2</sub> even though they were different materials. Considering that the organic percent of SiPS-N(CH<sub>3</sub>)<sub>3</sub>Cl was only 24.6%, and SiO<sub>2</sub> had strong and wide characteristic peaks, the chemical information from the organic components may be shielded. Moreover, the organic component was impregnated inside the SiO<sub>2</sub> and may be also responsible for such results. Similar phenomena were observed previously [25]. However, the characteristic peak of NO<sub>3</sub><sup>-</sup> appeared at 1386 cm<sup>-1</sup> in the FT-IR spectrum of SiPS-N(CH<sub>3</sub>)<sub>3</sub>NO<sub>3</sub> [41–43]. After the ReO<sub>4</sub><sup>-</sup> exchange, the characteristic peak of NO<sub>3</sub><sup>-</sup> disappeared and the characteristic peak of ReO<sub>4</sub><sup>-</sup> was observed at 916 cm<sup>-1</sup> [44–46]. These results demonstrated that the prepared SiPS-N(CH<sub>3</sub>)<sub>3</sub>Cl resin had the same anion exchange ability as traditional anion exchange resins.

SEM-EDS was used to examine the surface morphologies and the cross section of SiPS-N(CH<sub>3</sub>)<sub>3</sub>Cl. Fig. 6(a) and (b) show that SiPS-N(CH<sub>3</sub>)<sub>3</sub>Cl exhibited a uniform shape and smooth surface morphologies. The particle sizes were estimated to be in the range of 75–150 μm, which is consistent with SiO<sub>2</sub>. The magnified surface in Fig. 6(c) appears rugged and rich in mesopores. To determine whether the resin is implanted in the silica framework, EDS scanning was completed towards the cross section of SiPS-N(CH<sub>3</sub>)<sub>3</sub>Cl loaded with ReO<sub>4</sub><sup>-</sup>. Fig. 6(d)

shows that the adsorbed ReO<sub>4</sub><sup>-</sup> was uniformly distributed in the SiO<sub>2</sub> cross section; nitrogen was also detected. These results imply that the organic resin had been implanted into the SiO<sub>2</sub> framework by an *in-situ* solution polymerization method. In addition, diffusion from the solution to the inner pores was also observed, indicating the relation of particle size to diffusion distance. A small particle size likely leads to a short diffusion distance and thus improved adsorption kinetics.

### 3.2. Apparent volume and swelling rate

Organic resins are usually grafted with hydrophilic functional groups. They readily adsorb water and swell. High water swelling usually contributes to poor mechanical properties and high column pressure drops [24,39], which hampers chromatographic performance. In addition, the swelling rate often changes with salt concentration and type, thus making the resin volume inconstant. Therefore, the water swelling rate was estimated by the measurement of apparent volume in a dry and wet state. Fig. 7 shows that SiPS-N(CH<sub>3</sub>)<sub>3</sub>Cl exhibited almost the same apparent volume in the dry and wet state, suggesting that the water swelling rate was close to 0. The excellent anti-swelling property shows great promise in the chromatographic columns. In comparison, the apparent volume increased greatly from the dry state to the wet state for other resins such as D201, IRA900, and 732, indicating the large water swelling rate. Thus, we conclude that the implantation of the silica framework could effectively confine the water swelling of traditional organic resins.

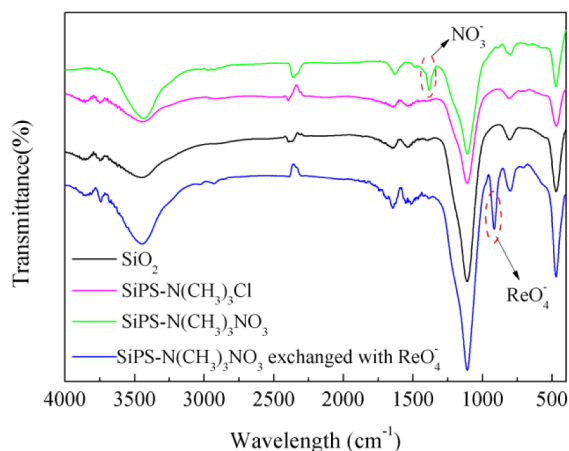


Fig. 5. The FT-IR spectrum of different samples.

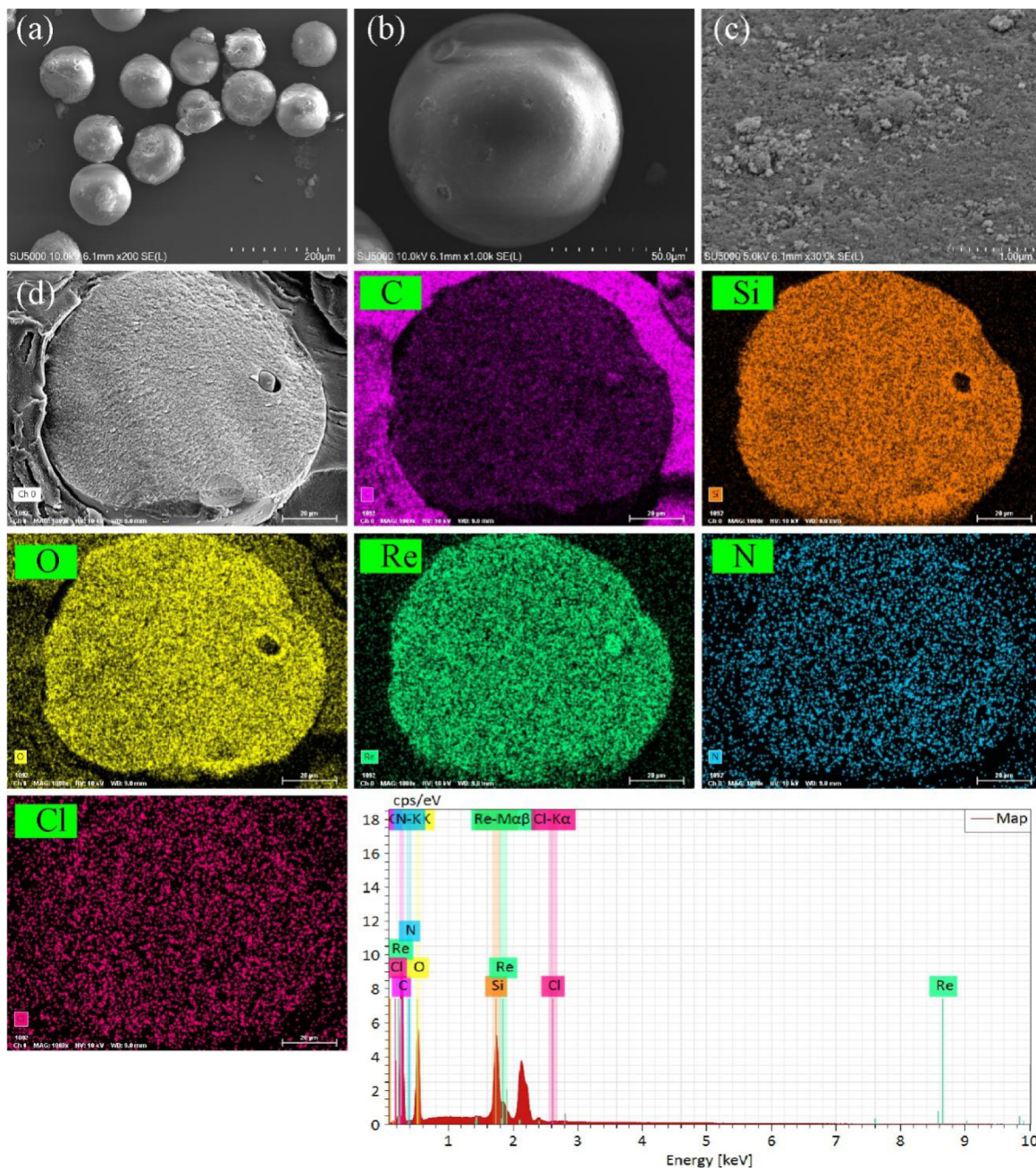


Fig. 6. Surface morphologies and EDS scanning towards the cross section of SiPS-N(CH<sub>3</sub>)<sub>3</sub>Cl.

### 3.3. Batch experiments

The lead speciation in different concentrations of hydrochloric acid was calculated by PHREEQC software to better understand the lead adsorption behavior of SiPS-N(CH<sub>3</sub>)<sub>3</sub>Cl. As shown in Fig. 8(a), the main lead species in hydrochloric acid included PbCl<sup>+</sup>, Pb<sup>2+</sup>, PbCl<sub>2</sub>, PbCl<sub>4</sub><sup>2-</sup>, and PbCl<sub>3</sub><sup>-</sup>. With increasing HCl concentration, the proportion of electropositive PbCl<sup>+</sup> and Pb<sup>2+</sup> gradually decreased while the PbCl<sub>3</sub><sup>-</sup> increased. For PbCl<sub>4</sub><sup>2-</sup>, the percent first increased and then decreased. At 1 M HCl, the proportion of lead species could be ordered as follows: PbCl<sup>+</sup> (41.3%) > PbCl<sub>2</sub> (24.9%) > PbCl<sub>3</sub><sup>-</sup>

(19.1%) > PbCl<sub>4</sub><sup>2-</sup> (11.2) > Pb<sup>2+</sup> (3.5), and the electronegative lead-chloride complexes merely occupied 30.3% of the total lead.

Fig. 8(b) investigated the adsorption behavior of SiPS-N(CH<sub>3</sub>)<sub>3</sub>Cl towards lead in different concentrations of HCl. The optimum concentration of HCl was 1.0 M for the adsorption of lead. A lower or higher HCl concentration would decrease the adsorption efficiency. The thermodynamic calculation suggested that the electronegative lead-chloride complexes occupied 30.3% of the total lead in 1 M HCl, but the maximum adsorption efficiency was lower than 20%. This indicates that competitive adsorption occurred between the electronegative lead-chloride complexes and the chloride anions. Furthermore, Fig. 8(a)

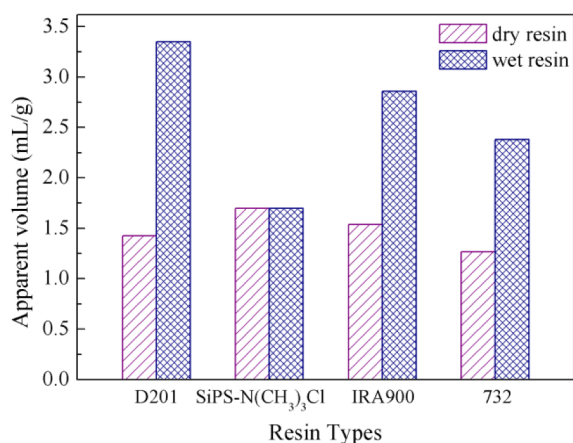


Fig. 7. Apparent volume of dry and wet resins per unit mass.

suggests the amount of anionic lead-chloride species always increased with the increasing concentration of HCl. However, the optimum efficiency was observed at the concentration of 1 M (HCl). It is speculated that the rising adsorption efficiency from 0 M (HCl) to 1.0 M (HCl) was mainly contributed by the increasing proportion of the anionic lead-chloride species, while the declining adsorption efficiency from 1.0 M (HCl) to 4.0 M (HCl) was resulted from the stronger competition from the chloride anions.

The separation of lead usually requires high concentrations of FeCl<sub>3</sub> due to the coprecipitation with lead cations. Therefore, the effect of FeCl<sub>3</sub> on the adsorption efficiency of lead was studied in 1 M HCl. Fig. 8(c) shows that the increasing concentration of FeCl<sub>3</sub> had minor effects on the adsorption efficiency of lead; this declined less than 3% even though the concentration of FeCl<sub>3</sub> approached 200 mM. The competitive adsorption with the chloride anion and the ferric-chloride complex anion may be responsible for the 3% decline in adsorption efficiency. In addition, this experiment indicated that SiPS-N(CH<sub>3</sub>)<sub>3</sub>Cl has a relatively higher affinity to the lead-chloride complex anion than the ferric-chloride complex anion and the chloride anion because the lead concentration was much lower than the ferric and chloride ion.

Fig. 8(d) illustrates the adsorption isotherm of lead in 1 M HCl solution. The adsorption efficiency rose gradually with the increase of initial lead concentration. Apparently, the loaded lead-chloride complex anions improved the adsorption performance (increased adsorption efficiency), indicating the occurrence of the synergistic adsorption mechanism. This kind of adsorption isotherm could be classified into “S” type [47], which could not be fitted with the frequently-used Langmuir and Freundlich equations. The “S” type adsorption isotherm revealed that the adsorption of lead-chloride complex anion faced an intense competition by the chloride anion for the active sites, which was also supported by Fig. 8(b) and (c). The maximum adsorption amount towards lead exceeded 13 mg/g.

The adsorption kinetics were investigated in Fig. 8(e) and (f). As seen in Fig. 8(e), the adsorption requires 30 min to achieve the equilibrium state at a concentration of 500 mg (Pb<sup>2+</sup>)/L. The equilibrium time shortens to 5 min at a higher concentration of 1000 mg (Pb)/L. These results suggested that the SiPS-N(CH<sub>3</sub>)<sub>3</sub>Cl had superior adsorption kinetics towards lead in HCl solution, and confirmed the formation of the synergistic adsorption, which reduced the equilibrium time at a higher concentration of lead. The intra-particle diffusion model was used to fit the experimental data to distinguish different kinetic regions [48]. As shown in Fig. 8(f), the adsorption process can be separated into

three stages. The first linear stage marked with the red color could be attributed to the adsorption of lead on the external or macropores of SiPS-N(CH<sub>3</sub>)<sub>3</sub>Cl, after diffusion through the boundary layer [49]; The second linear stage marked with the blue color corresponded to the diffusion through the mesopores; And the third stage marked with the black color is the equilibrium stage. These suggested that the adsorption of lead in 1 M HCl covered the intra-particle diffusion and intra-particle adsorption activities. The first stage at 1000 mg/L occurred less than 3 min, so it was not observed. The parameters fitted by the intra-particle model were listed in Table 3. The value of  $K_2$  for 1000 mg/L was larger than that for 500 mg/L, indicating a more rapid diffusion rate. The value of  $K_3$  is close to 0, corresponding to adsorption equilibrium. The pseudo first-order kinetic model and the pseudo second-order kinetic model were also employed to fit the experimental data, of which the results were shown in Fig. S2 and Table S2. The R square values and the fitting results of PSO were found to be better than that of PFO, implying that the adsorption activities were dominated by chemical reactions.

### 3.4. Column experiments for the establishment of the separation process

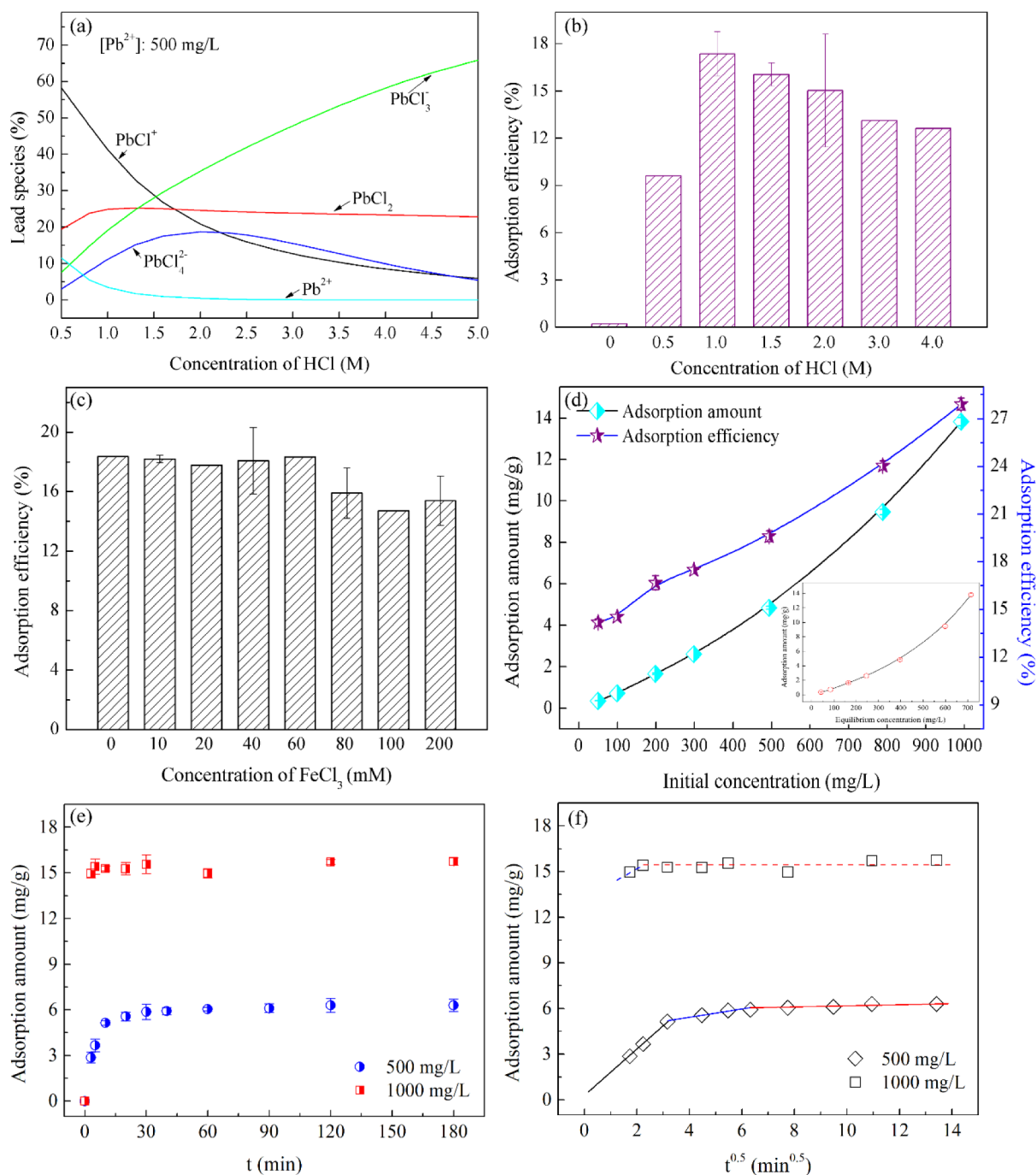
Static adsorption efficiency of SiPS-N(CH<sub>3</sub>)<sub>3</sub>Cl towards lead was approximately 18% in 1 M HCl solution, and thus column separation was the exclusive method to realize the quantitative recovery of lead, because the dynamic adsorption in columns could be regarded as the combination of numerous static adsorption processes. The breakthrough curve in 1 M HCl was first studied. As shown in Fig. 9(a), lead was effectively immobilized by SiPS-N(CH<sub>3</sub>)<sub>3</sub>Cl when the volume of effluent was less than 30 mL. After that, the concentration of lead climbed gradually and then approached the feeding concentration. Considering that the adsorbed lead-chloride anions improve the adsorption performance of SiPS-N(CH<sub>3</sub>)<sub>3</sub>Cl, a higher concentration may lead to a better result, i.e., more lead is adsorbed. However, the volume of influent was still controlled within 25 mL for the recovery of lead, which also coincided with the real situation.

Fig. 9(b) shows the elution results of 1 M HCl solution to the lead-loaded columns. A small amount of lead was eluted from the HCl, and more HCl will contribute to the desorption of lead, due to the intense competition between chloride anions and lead-chloride complex anions. To obtain a high recovery rate, the volume of HCl used for the elution should be controlled within 10 mL.

Fig. 9(c) details the effect of flow speed on the lead recovery. The flow speed had minor effects on the lead recovery rate. Flow speeds of 1.0 mL/min and 2.0 mL/min led to consistent adsorption/desorption curves. A higher rate of 4.0 mL/min showed the similar adsorption curves, but the concentration distribution of lead became more dispersive. However, lead was concentrated within 15 mL of effluent from the volume point of 30 to 45 mL regardless of the difference in flow speed. 2.0 mL/min was finally selected as the optimum flow speed for the experiments to protect the soft tubes.

The mixed solution containing 90 mM of FeCl<sub>3</sub> was also allowed to flow through the regenerated and pretreated column. The results are shown in Fig. 9(d) and confirmed that lead in the mixed solution was still effectively immobilized by the column even though it co-existed with high concentration of FeCl<sub>3</sub>. In addition, the change in solution color suggested that the collected solution (the last four tubes) had few ferric cations, indicating that lead could be separated from other cations by this method and material under real conditions. Table S3 lists the chemical yield of lead obtained in Fig. 9(c) and (d). Generally, the flow speed and the co-existence of FeCl<sub>3</sub> had minor effects on the chemical yield of lead in 1 M HCl solution, because the chemical yields of lead all





**Fig. 8.** Lead species distribution (a) and the effects of HCl concentration (b), FeCl<sub>3</sub> concentration (c), initial lead concentration (d), and the contacting time (e–f) on the adsorption lead adsorption performance of SiPS-N(CH<sub>3</sub>)<sub>3</sub>Cl. Experimental conditions: (b)  $t = 1$  h, [Pb<sup>2+</sup>] = 500 mg/L; (c)  $t = 1$  h, [Pb<sup>2+</sup>] = 500 mg/L, [HCl] = 1.0 M; (d)  $t = 1$  h, [HCl] = 1.0 M; (e–f) [HCl] = 1.0 M.

**Table 3**

Intra-particle parameters for the lead adsorption onto SiPS-N(CH<sub>3</sub>)<sub>3</sub>Cl.

Concentration	$K_1$	$K_2$	$K_3$	$C_1$	$C_2$	$C_3$	$R_1^2$	$R_2^2$	$R_3^2$
500	1.597	0.2560	0.0550	0.0954	4.379	5.605	0.9999	0.9324	0.8520
1000	–	0.9031	0.0354	–	13.40	15.19	–	1.000	0.1381

Note: the unit of Concentration,  $K$  and  $C$  are mg/L, mg/g/min<sup>0.5</sup> and mg/g, respectively.

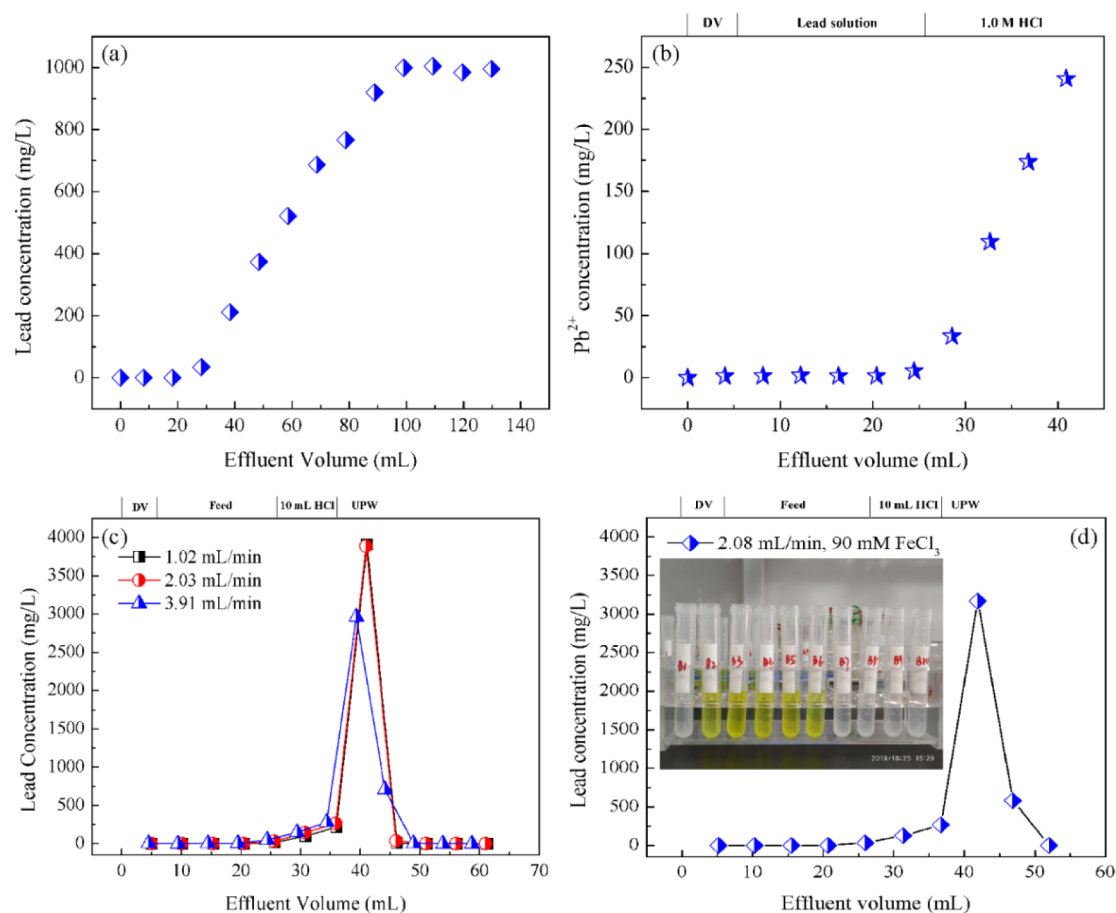


Fig. 9. (a) Breakthrough curve of lead in 1.0 M HCl; (b) Effect of HCl (1.0 M) volume on the lead concentration in the effluent; (c) Effect of flow speed on the chemical yield of lead; (d) effect of FeCl<sub>3</sub> on the chemical yield of lead. Experimental conditions:  $m(\text{resin}) = 3.3579 \text{ g}$ , column  $\phi \times h = 5 \text{ mm} \times 30 \text{ cm}$ , bed volume = 5.89 mL,  $[\text{Pb}^{2+}]_{\text{feed}} = 1000 \text{ mg/L}$  (These were common); (a) Flow speed = 2.0 mL/min; (b) Flow speed = 1.0 mL/min.

exceeded 95% under different conditions.

Based on the results mentioned-above, a separation process integrated the optimum operation parameters: the mixed solution containing  $^{210}\text{Pb}$  and its stable isotope  $^{207}\text{Pb}$  (should be less than 25 mL) was first allowed to flow through the column ( $\phi \times h = 5 \text{ mm} \times 30 \text{ cm}$ ) packed with SiPS-N(CH<sub>3</sub>)<sub>3</sub>Cl at a speed of 2.0 mL/min; Next, 10 mL of 1 M HCl solution was pumped to elute the residual ions; As followed, 15 mL of UPW was fed to desorb the lead, and the automatic fraction collector started to collect simultaneously. For the convenience of comparison, Table 4 lists the technological parameters for the different recovery processes. The parameters of this work were superior to those reported by others [19,21,50]. The separation time could be controlled within 30 min while those of others were much longer. The retention time of solution for SiPS-N(CH<sub>3</sub>)<sub>3</sub>Cl is calculated as about 3 min, which is the least among these materials. As comparison, the retention time of solution for 201 × 7 is about 66 min and 330 min for adsorption and

desorption, respectively. Therefore, it can be concluded that SiPS-N(CH<sub>3</sub>)<sub>3</sub>Cl has a fast adsorption kinetics.

The process was finally tested by the Radiation-Environment Management and Monitoring Station of Guangxi Zhuang Automatic Region with real environmental water samples. The results were shown in Table 5 and compared with those obtained by 201 × 7 using the standard process described in reference [21]. Here, two environmental water samples A and B were collected near a uranium mining site in Guangxi Province and duplicated twice. It was found that the chemical yield of lead for the two water samples all exceeded 95% for 201 × 7 and SiPS-N(CH<sub>3</sub>)<sub>3</sub>Cl. The radioactivity concentrations obtained by SiPS-N(CH<sub>3</sub>)<sub>3</sub>Cl were 5.65 and 25.4 mBq/L for samples A and B, respectively, which were close to those obtained by 201 × 7 based on the industrial standard. These demonstrates that the developed silica-supported anion exchange resin and the matched process could be used to determine  $^{210}\text{Pb}$  in environmental samples.

Table 4

Comparison of technological parameters among different recovery processes.

Ref.	Resin type	Column dimension	$V_{\text{feeding}}$ (mL)	$V_{\text{HCl}}$ (mL)	$V_{\text{UPW}}$ (mL)	$\nu$ (mL/min)
[19]	201 × 7	13 mm × 25 cm	50	10 ~ 20	40	0.5 <sup>a</sup> /0.1 <sup>d</sup>
[50]	BIO-RAG-AG 1-X4	13 mm × 25 cm	24	35	50	0.5 <sup>a</sup> /0.5 <sup>d</sup>
[21]	201 × 7	Not mentioned	14–17	140	80	0.1 <sup>a</sup> /0.1 <sup>d</sup>
This work	SiPS-N(CH <sub>3</sub> ) <sub>3</sub> Cl	5 mm × 30 cm	14–25	10	15	2.0 <sup>a</sup> /2.0 <sup>d</sup>

<sup>a</sup> denotes the flow speed for adsorption; <sup>d</sup> denotes the flow speed for washing and desorption;  $V$  denotes the volume;  $\nu$  represents flow speed.

**Table 5**  
The radioactivity concentration of  $^{210}\text{Pb}$  in different water samples collected in Guangxi province.

Collecting Location	Sample type	Added lead carrier (mg)	Lead recovered (mg)	Chemical yield (%)	Measured radioactivity concentration of $^{210}\text{Pb}$ (mBq/L)	Resin used	Separation process
A 脚古冲	Lake water	9.750	10.430	107	5.8	201 × 7	Industrial standard
B 总排口	Waste water	9.750	10.140	101	27.7	201 × 7	Industrial standard
A 脚古冲	Lake water	9.750	9.848	104	5.65	SiPS-N ( $\text{CH}_3$ ) <sub>3</sub> Cl	This work
B 总排口	Waste water	9.750	9.653	99	25.4	SiPS-N ( $\text{CH}_3$ ) <sub>3</sub> Cl	This work

#### 4. Conclusion

This work developed a novel silica-supported anion exchange resin with superior exchange kinetics and the same chemical performance as traditional anion exchange resin. Compared to typical anion exchange resins, such as D201 and IRA900, the SiPS-N( $\text{CH}_3$ )<sub>3</sub>Cl had smaller particle sizes (75–150  $\mu\text{m}$ ), a much lower water swelling rate (0%), and a larger specific surface area (59.03  $\text{m}^2/\text{g}$ ). The maximum anion exchange capacity resulted from quaternary amine groups was determined to be 1.0 mmol ( $\text{Cl}^-$ )/g.

Batch results suggested that lead adsorption by SiPS-N( $\text{CH}_3$ )<sub>3</sub>Cl faced strong competition from the chloride anion, leading to low adsorption efficiencies in the HCl solution even at the optimum concentration (1.0 M). The concentration of lead was found related to the equilibrium time due to the occurrence of synergistic adsorption indicated by the “S” type adsorption isotherm. The equilibration time required for 500 mg ( $\text{Pb}^{2+}$ )/L and 1000 mg ( $\text{Pb}^{2+}$ )/L was about 30 min and 5 min, respectively. The concentration of co-existing  $\text{FeCl}_3$  had little effect on the adsorption efficiency of lead, which declined less than 3%, with the  $\text{FeCl}_3$  concentration reaching to 200 mM. The adsorption isotherm of SiPS-N( $\text{CH}_3$ )<sub>3</sub>Cl suggested that the adsorption efficiency increased gradually with increasing lead equilibrium concentration. This is different from the commonly-observed adsorption isotherms and indicated the occurrence of synergistic adsorption.

The column results suggested that the feeding volume of lead solution and HCl solution (for eluting the residual ions) should be strictly controlled due to the important effect on the chemical yield of lead, and the lead recovery could be performed at a speed of 4.0 mL/min regardless of the co-existing high concentrations of  $\text{FeCl}_3$ . Based on these results, a separation process integrating this novel material and the matched parameters was developed and tested with actual environmental water samples. The results showed that SiPS-N( $\text{CH}_3$ )<sub>3</sub>Cl could quickly separate the lead from the mixed solution derived from environmental water samples with chemical yields exceeding 95%; the time was controlled to within 30 min. Furthermore, the radioactivity concentrations obtained by this separation process were quite close to those obtained by 201 × 7 using the standard separation process.

In conclusion, SiPS-N( $\text{CH}_3$ )<sub>3</sub>Cl is an excellent alternative to traditional anion exchange resins. This material and protocol show promise and significance in the determination of  $^{210}\text{Pb}$  in environmental samples.

#### Declaration of Competing Interest

The authors declare that they have no known competing financial interests or personal relationships that could have appeared to influence the work reported in this paper.

#### Acknowledgements

This work was supported by the National Natural Science Foundation of China [grant number 21866007] and the Open Foundation of Guangxi Key Laboratory of Processing for Nonferrous Metals, and Featured Materials of Guangxi University (grant number

gxysof1808). The authors would like to acknowledge the help of Lingyu Lu in the Radiation-Environment Management and Monitoring Station of Guangxi Zhuang Autonomous Region.

#### Appendix A. Supplementary data

Supplementary data to this article can be found online at <https://doi.org/10.1016/j.cej.2020.125300>.

#### References

- [1] G. Jia, Simultaneous determination of  $^{210}\text{Po}$  and  $^{210}\text{Pb}$  in solid samples: A new method for  $^{210}\text{Pb}$  determination, *Appl. Radiat. Isot.* 137 (2018) 12–17, <https://doi.org/10.1016/j.apradiso.2018.02.019>.
- [2] N. Aslan, G. Özçayan, Adsorptive removal of lead-210 using hydroxyapatite nanopowders prepared from phosphogypsum waste, *J. Radioanal. Nucl. Chem.* 319 (2019) 1023–1028, <https://doi.org/10.1007/s10967-018-6388-x>.
- [3] E.-S. Ibrahim Shabana, M. Mohammad, A. Taher Qutub, Kinsara Accumulation of Lead-210 and Polonium-210 in the Groundwater of Wadi Nu'man, Mecca Province, *Arab. J. Sci. Eng.* 41 (2016) 4217–4224, <https://doi.org/10.1007/s13369-016-2161-z>.
- [4] N.H. Harley, P. Chittaporn, I.M. Fisenne, P. Perry,  $^{222}\text{Rn}$  decay products as tracers of indoor and outdoor aerosol particle size, *J. Environ. Radioactiv.* 51 (2000) 27–35, [https://doi.org/10.1016/S0265-931X\(00\)00042-4](https://doi.org/10.1016/S0265-931X(00)00042-4).
- [5] M.-A. Mélières, M. Pourchet, S. Richard, Surface air concentration and deposition of lead-210 in French Guiana: two years of continuous monitoring, *J. Environ. Radioactiv.* 66 (2003) 261–269, [https://doi.org/10.1016/S0265-931X\(02\)00111-X](https://doi.org/10.1016/S0265-931X(02)00111-X).
- [6] M. Baskaran, Po-210 and Pb-210 as atmospheric tracers and global atmospheric Pb-210 fallout: a review, *J. Environ. Radioactiv.* 102 (2011) 500–513, <https://doi.org/10.1016/j.jenvrad.2010.10.007>.
- [7] Y. Ebaid, A. Khater, Determination of  $^{210}\text{Pb}$  in environmental samples, *J. Radioanal. Nucl. Chem.* 270 (2006) 609–619, <https://doi.org/10.1007/s10967-006-0470-5>.
- [8] K. Meusbürger, P. Porto, L. Mabit, C. La Spada, L. Arata, C. Alewell, Excess Lead-210 and Plutonium-239+240: two suitable radiogenic soil erosion tracers for mountain grassland sites, *Environ. Res.* 160 (2018) 195–202, <https://doi.org/10.1016/j.envres.2017.09.020>.
- [9] H. Yang, P.G. Appleby, Use of lead-210 as a novel tracer for lead (Pb) sources in plants, *Sci. Rep.* 6 (2016) 21707, <https://doi.org/10.1038/srep21707>.
- [10] G.J. Ham, B.T. Wilkins, L.W. Ewers,  $^{210}\text{Pb}$ ,  $^{210}\text{Po}$ ,  $^{226}\text{Ra}$ , U and Th in Arable Crops and Ovine Liver: variations in Concentrations in the United Kingdom and Resultant Doses, *Radiat. Prot. Dosim.* 93 (2001) 151–159, <https://doi.org/10.1093/oxfordjournals.rpd.a006423>.
- [11] Z. Pietrzak-Flis, E. Chrzanowski, S. Dembinska, Intake of  $^{226}\text{Ra}$ ,  $^{210}\text{Pb}$  and  $^{210}\text{Po}$  with food in Poland, *Sci. Total. Environ.* 203 (1997) 157–165, [https://doi.org/10.1016/S0048-9697\(97\)00144-7](https://doi.org/10.1016/S0048-9697(97)00144-7).
- [12] J.L. Smith-Briggs, E.J. Bradley, M.D. Potter, The ratio of lead-210 to polonium-210 in U.K. diet, *Sci. Total. Environ.* 54 (1986) 127–133, [https://doi.org/10.1016/0048-9697\(86\)90260-3](https://doi.org/10.1016/0048-9697(86)90260-3).
- [13] L.-J. Pan, G.-B. Yu, Z. Chen, L.-S. Sheng, X.G. Xu, A modified sampling preparation method for rapid determination of Pb-210 radioactivity in plants in China using crown ether and liquid scintillation counting of beta particles, *J. Radioanal. Nucl. Chem.* 317 (2018) 565–570, <https://doi.org/10.1007/s10967-018-5919-9>.
- [14] J.P. Bolivar, R. García-Tenorio, M. García-León, Radioactive impact of some phosphogypsum piles in soils and salt marshes evaluated by  $\gamma$ -ray spectrometry, *Appl. Radiat. Isot.* 47 (1996) 1069–1075, [https://doi.org/10.1016/S0969-8043\(96\)00108-X](https://doi.org/10.1016/S0969-8043(96)00108-X).
- [15] J. Paatero, J. Hatakka, R. Mattsson, Y. Viisanen, Analysis of Daily  $^{210}\text{Pb}$  Air Concentrations in Finland, 1967–1996, *Radiat. Prot. Dosim.* 77 (1998) 191–198, <https://doi.org/10.1093/oxfordjournals.rpd.a032310>.
- [16] D.I. Strumińska-Parulska, G. Olszewski, J. Falandysz,  $^{210}\text{Po}$  and  $^{210}\text{Pb}$  bioaccumulation and possible related dose assessment in parasol mushroom (*Macrolepiota procera*), *Environ. Sci. Pollut. R.* 24 (2017) 26858–26864, <https://doi.org/10.1007/s11356-017-0458-4>.
- [17] D. Desideri, F. Guerra, M.A. Meli, C. Testa, Determination of  $^{210}\text{Pb}$  in sediments by extraction chromatography, *J. Radioanal. Nucl. Chem.* 200 (1995) 385–396, <https://doi.org/10.1007/bf02162880>.

- [18] E.E. Santos, D.C. Lauria, E.C.S. Amaral, E.R. Rochedo, Daily ingestion of  $^{232}\text{Th}$ ,  $^{238}\text{U}$ ,  $^{226}\text{Ra}$ ,  $^{228}\text{Ra}$  and  $^{210}\text{Pb}$  in vegetables by inhabitants of Rio de Janeiro City, J. Environ. Radioactiv. 62 (2002) 75–86, [https://doi.org/10.1016/S0265-931X\(01\)00152-7](https://doi.org/10.1016/S0265-931X(01)00152-7).
- [19] G. Jia, M. Belli, S. Liu, U. Sansone, C. Xu, S. Rosamilia, X. Xiao, S. Gaudino, L. Chen, H. Yang, The fractionation and determination procedures for the speciation of  $^{210}\text{Pb}$  and  $^{210}\text{Po}$  in soil samples, Anal. Chim. Acta 562 (2006) 51–58, <https://doi.org/10.1016/j.aca.2006.01.058>.
- [20] G. Jia, M. Belli, M. Blasi, A. Marchetti, S. Rosamilia, U. Sansone,  $^{210}\text{Pb}$  and  $^{210}\text{Po}$  determination in environmental samples, Appl. Radiat. Isot. 53 (2000) 115–120, [https://doi.org/10.1016/S0969-8043\(00\)00121-4](https://doi.org/10.1016/S0969-8043(00)00121-4).
- [21] P. Liu, J. Shan, D. Xiao, F. Xiao, H. Wang, J. Shu, H. Yang, The Specific Activity and Balance's Measuring of  $^{226}\text{Ra}$ ,  $^{210}\text{Pb}$  and  $^{210}\text{Po}$  in Hengyang Specific Water Environment, Nucl. Electron. Detect. Technol. 38 (2018) 43–59.
- [22] X. Li, Q. Zhao, Q. Wang, M. Luo, Application of  $^{210}\text{Pb}$  Analysis Method in Aerosol Determination of Chengdu, Sichuan Environment. 36 (2017) 142–146.
- [23] C. Xiao, M.A. Silver, S. Wang, Metal-organic frameworks for radionuclide sequestration from aqueous solution: a brief overview and outlook, Dalton Trans. 46 (2017) 16381–16386, <https://doi.org/10.1039/C7DT03670A>.
- [24] L. Chen, X. Yin, Q. Yu, L. Siming, F. Meng, S. Ning, X. Wang, Y. Wei, Rapid and selective capture of perhenate anion from simulated groundwater by a mesoporous silica-supported anion exchanger, Microporous Mesoporous Mater. 274 (2019) 155–162, <https://doi.org/10.1016/j.micromeso.2018.07.029>.
- [25] L. Chen, Y. Chen, X. Wang, Y. Wei, L. He, F. Tang, A novel silica-based anion exchange resin used for removing uranium from drinking water, J. Radioanal. Nucl. Chem. 314 (2017) 2569–2578.
- [26] L. Zhu, D. Sheng, C. Xu, X. Dai, M.A. Silver, J. Li, P. Li, Y. Wang, Y. Wang, L. Chen, Identifying the Recognition Site for Selective Trapping of  $^{99}\text{TcO}_4^-$  in a Hydrolytically Stable and Radiation Resistant Cationic Metal-Organic Framework, J. Am. Chem. Soc. 139 (2017) 14873–14876, <https://doi.org/10.1021/jacs.7b08632>.
- [27] R.J. Drout, K. Otake, A.J. Howarth, T. Islamoglu, L. Zhu, C. Xiao, S. Wang, O.K. Farha, Efficient Capture of Perrhenate and Pertechnate by a Mesoporous Zr Metal-Organic Framework and Examination of Anion Binding Motifs, Chem. Mater. 30 (2018) 1277–1284, <https://doi.org/10.1021/acs.chemmater.7b04619>.
- [28] D. Sheng, L. Zhu, C. Xu, C. Xiao, Y. Wang, Y. Wang, L. Chen, J. Diwu, J. Chen, Z. Chai, Efficient and Selective Uptake of  $\text{TeO}_4^{2-}$  by a Cationic Metal-Organic Framework Material with Open  $\text{Ag}^+$  Sites, Environ. Sci. Technol. 51 (2017) 3471, <https://doi.org/10.1021/acs.est.7b00339>.
- [29] D. Sheng, L. Zhu, X. Dai, C. Xu, P. Li, C.I. Pearce, C. Xiao, J. Chen, R. Zhou, T. Duan, O.K. Farha, Z. Chai, S. Wang, Successful Decontamination of  $^{99}\text{TcO}_4^-$  in Groundwater at Legacy Nuclear Sites by a Cationic Metal-Organic Framework with Hydrophobic Pockets, Angew. Chem. Int. Ed. 58 (2019) 4968–4972, <https://doi.org/10.1002/anie.201814640>.
- [30] J. Li, X. Dai, L. Zhu, C. Xu, D. Zhang, M.A. Silver, P. Li, L. Chen, Y. Li, D. Zuo, H. Zhang, C. Xiao, J. Chen, J. Diwu, O.K. Farha, T.E. Albrecht-Schmitt, Z. Chai, S. Wang,  $^{99}\text{TcO}_4^-$  remediation by a cationic polymeric network, Nat Commun 9 (2018) 3007, <https://doi.org/10.1038/s41467-018-05380-5>.
- [31] Z. Zhang, Z. Dong, X. Wang, D. Ying, F. Niu, X. Cao, Y. Wang, R. Hua, Y. Liu, X. Wang, Ordered mesoporous polymer-carbon composites containing amidoxime groups for uranium removal from aqueous solutions, Chem. Eng. J. 341 (2018) 208–217, <https://doi.org/10.1016/j.cej.2018.02.044>.
- [32] Y. Wang, H. Gao, Compositional and structural control on anion sorption capability of layered double hydroxides (LDHs), J. Colloid Interface Sci. 301 (2006) 19–26, <https://doi.org/10.1016/j.jcis.2006.04.061>.
- [33] G. Sheng, Y. Tang, W. Linghu, L. Wang, J. Li, H. Li, X. Wang, Y. Huang, Enhanced immobilization of  $\text{ReO}_4^-$  by nanoscale zerovalent iron supported on layered double hydroxide via an advanced XAFS approach: Implications for  $\text{TeO}_4^-$  sequestration, Appl. Catal. B-Environ. 192 (2016) 268–276, <https://doi.org/10.1016/j.apcatb.2016.04.001>.
- [34] S. Wang, E.V. Alekseev, J. Diwu, W.H. Casey, B.L. Phillips, W. Depmeier, T.E. Albrecht-Schmitt, NDTB-1: A Supertetrahedral Cationic Framework That Removes  $\text{TeO}_4^-$  from Solution, Angew. Chem. Int. Ed. 49 (2010) 1057–1060, <https://doi.org/10.1002/anie.200906397>.
- [35] S. Wang, P. Yu, B.A. Purse, M.J. Orta, J. Diwu, W.H. Casey, B.L. Phillips, E.V. Alekseev, W. Depmeier, D.T. Hobbs, T.E. Albrecht-Schmitt, Selectivity, Kinetics, and Efficiency of Reversible Anion Exchange with  $\text{TeO}_4^-$  in a Supertetrahedral Cationic Framework, Adv. Funct. Mater. 22 (2012) 2241–2250, <https://doi.org/10.1002/adfm.2011103081>.
- [36] Y. Xiong, X. Cui, P. Zhang, Y. Wang, Z. Lou, W. Shan, Improving Re(VII) Adsorption on Diisobutylamine-Functionalized Graphene Oxide, ACS Sustain. Chem. Eng. 5 (2016) 1010–1018, <https://doi.org/10.1021/acssuschemeng.6b02322>.
- [37] J.H. Chen, H.T. Xing, H.X. Guo, W. Weng, S.R. Hu, S.X. Li, Y.H. Huang, X. Sun, Z.B. Su, Investigation on the adsorption properties of Cr(VI) ions on a novel graphene oxide (GO) based composite adsorbent, J. Mater. Chem. A 2 (2014) 12561–12570, <https://doi.org/10.1039/C4TA02004A>.
- [38] C. He, Z. Yang, J. Ding, Y. Chen, X. Tong, Y. Li, Effective removal of Cr(VI) from aqueous solution by 3-aminopropyltriethoxysilane-functionalized graphene oxide, Colloid Surface A 520 (2017) 448–458, <https://doi.org/10.1016/j.colsurfa.2017.01.086>.
- [39] X. Wang, Z. Ye, L. Chen, Q. Zheng, C. Liu, S. Ning, A. Khayambashi, Y. Wei, Microporous silica-supported cation exchanger with superior dimensional stability and outstanding exchange kinetics, and its application in element removal and enrichment, React. Funct. Polym. 142 (2019) 87–95, <https://doi.org/10.1016/j.reactfunctpolym.2019.06.007>.
- [40] Z. Ye, X. Yin, L. Chen, X. He, Z. Lin, C. Liu, S. Ning, X. Wang, Y. Wei, An integrated process for removal and recovery of Cr(VI) from electroplating wastewater by ion exchange and reduction-precipitation based on a silica-supported pyridine resin, J. Clean. Prod. 236 (2019) 117631, <https://doi.org/10.1016/j.jclepro.2019.117631>.
- [41] Y. Peng, F. Annabi-Bergaya, T. Qi, M. Fan, Z. Liu, J. Zhu, H. He, T. Chen, A combined study by XRD, FTIR, TG and HRTEM on the structure of delaminated Fe-intercalated/pillared clay, J. Colloid Interface Sci. 324 (2008) 142–149, <https://doi.org/10.1016/j.jcis.2008.04.076>.
- [42] M. Islam, R. Patel, Nitrate sorption by thermally activated Mg/Al chloride hydroxalite-like compound, J. Hazard. Mater. 169 (2009) 524–531, <https://doi.org/10.1016/j.jhazmat.2009.03.128>.
- [43] Q. Hu, N. Chen, C. Feng, W.W. Hu, Nitrate adsorption from aqueous solution using granular chitosan- $\text{Fe}^{3+}$  complex, Appl. Surf. Sci. 347 (2015) 1–9, <https://doi.org/10.1016/j.apsusc.2015.04.049>.
- [44] I.A. Miniakhmetov, S.A. Semenov, V.Y. Musatova, A.M. Reznik, Solvent extraction of rhenium with N-(2-hydroxy-5-nonylbenzyl)- $\beta$ -hydroxyethylmethylamine, Russ. J. Inorg. Chem. 58 (2013) 1380–1382, <https://doi.org/10.1134/s0036023613110144>.
- [45] M. Jia, H. Cui, W. Jin, L. Zhu, Y. Liu, J. Chen, Adsorption and separation of rhenium (VII) using N-ethylimidazolium functionalized strong basic anion exchange resin, J. Chem. Technol. Biotechnol. 88 (2013) 437–443, <https://doi.org/10.1002/jctb.3904>.
- [46] B.M. Marković, Z.M. Vuković, V.V. Spasojević, V.B. Kusigerski, V.B. Pavlović, A.E. Onjia, A.B. Nastasović, Selective magnetic GMA based potential sorbents for molybdenum and rhenium sorption, J. Alloys Compd. 705 (2017) 38–50, <https://doi.org/10.1016/j.jallcom.2017.02.108>.
- [47] C.H. Giles, D. Smith, A. Huitson, A general treatment and classification of the solute adsorption isotherm. I. Theoretical, J. Colloid Interface Sci. 47 (1974) 755–765, [https://doi.org/10.1016/0021-9797\(74\)90252-5](https://doi.org/10.1016/0021-9797(74)90252-5).
- [48] W.J. Weber, J.C. Morris, Kinetics of adsorption on carbon from solution, J. Sanit. Eng. Divis. 89 (1963) 31–60.
- [49] E. Fuentes-Quezada, E. de la Llave, E. Halac, M. Jobbágy, F.A. Viva, M.M. Bruno, H.R. Corti, Bimodal mesoporous hard carbons from stabilized resorcinol-formaldehyde resin and silica template with enhanced adsorption capacity, Chem. Eng. J. 360 (2019) 631–644, <https://doi.org/10.1016/j.cej.2018.11.235>.
- [50] G. Jia, G. Torri, Determination of  $^{210}\text{Pb}$  and  $^{210}\text{Po}$  in soil or rock samples containing refractory matrices, Appl. Radiat. Isot. 65 (2007) 1–8, <https://doi.org/10.1016/j.apradiso.2006.05.007>.